Simulation of Photon Thermalization in a Single-photon Detector on the Basis of CeB_6 Thermoelectric Sensor

A.S. Kuzanyan, V.R. Nikoghosyan and A.A. Kuzanyan

Material Science Lab., Institute for Physical Research, Ashtarak-2, 0203, Republic of Armenia
A.S. Kuzanyan: akuzanyan@yahoo.com

ABSTRACT

Interest in single-photon detectors (SPD) has recently increased dramatically, due to many novel applications. The most developed SPD are currently based on superconductors. Following the theory, thermoelectric single-photon detectors (TSPD) can compete with superconducting detectors. The operational principle of TSPD is based on photon absorption by absorber as a result of which a temperature gradient is generated across the sensor. In this work we present the results of computer modeling of the TSPD. We observe the processes of heat distribution after absorption of a photon of 1 keV (X-rays), 100 eV (hard UV), 10 eV (UV) and 1 eV (IR) energy in different areas of the absorber for different geometries of absorber and sensor. The time dependence of the temperature difference between the ends of the thermoelectric bridge and electric potential appearing across the sensor are calculated. The results of calculations show that it is realistic to detect single photons from IR to X-ray and determine their energy. Count rates up to 100 GHz can be achieved.

Keywords: simulation, single-photon, thermoelectric detector, heat distribution

1 INTRODUCTION

Intensive development of science and engineering requires new generations of devices for precise measurements. Interest in single-photon detectors (SPDs) has recently increased dramatically, due to many novel applications in various research fields, such as quantum communication, quantum cryptography, space astronomy, chemical analysis, particle physics, medical applications, traditional and quantum-enabled metrology and others [1]. The most developed SPDs are currently based on superconductors [2]. Over the last fifteen years superconducting nanowire single-photon detectors (SNSPD) are actively investigated because of their high system detection efficiency, low dark count rate, high counting rate and timing resolution [3]. Following the theory, thermoelectric detectors (TSPD) can compete with superconducting detectors [4] and thermoelectric nanowire single-photon detector (TNSPD) with superconducting nanowire single-photon detectors [5].

Sensitivity of thermoelectric devices to single photons is determined by the signal/noise ratio, the consideration of which gives acceptable energy resolution. Thus, to provide the energy resolution of 1 eV at a single-photon absorption, the thermoelectric material must have a Seebeck coefficient of ~ 100 μV/K. Materials with a higher Seebeck coefficient are abundant, but the point is that in order to achieve the required signal/noise ratio, the detector must operate at very low temperatures. One of the well-known low temperature thermoelectric materials is the gold with iron impurities. However, in our opinion, cerium hexaboride (CeB_6) is more promising [6, 7].

2 METHODOLOGY

2.1. Thermoelectric single-photon detector

The operational principle of TSPD is based on photon absorption by absorber as a result of which a temperature gradient is generated across the sensor. Photon detection becomes possible by measuring the potential, emerging between the two absorbers. The scheme of the TSPD sensitive element is given on Fig. 1. In this work we present the results of computer modeling of the TNSPD. We observe the processes of heat distribution after absorption of a photon of 1 eV (IR), 10 eV (UV), 100 eV (hard UV) and 1 keV(X-rays) energy in different areas of the absorber (points N, M and F in Fig. 1) for different geometries of tungsten absorbers and CeB6 sensor. Figure 1 also shows the directions of coordinate

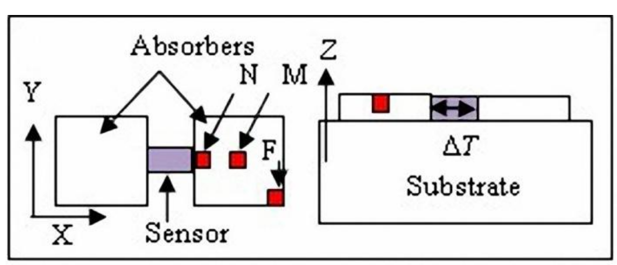

Fig. 1. The detection pixel of TSPD.

axes: x is parallel to the axis of symmetry of the sensor (corresponding to the length of geometric shapes), y is perpendicular to x (width), z is perpendicular to x, y and to the substrate surface (height).

2.2. Computing technique

The calculations were based on the heat conduction equation. For simplicity of calculations in a first approximation, the phonon contribution to the heat capacity is not taken into account. The time dependence of the temperature difference between the ends of the thermoelectric bridge (ΔT) and electric potential (ΔU) appearing across the sensor are calculated. The calculations were carried out by the matrix method for differential equations. The operating temperature of the detector was taken to be 9 K. The materials used have the parameters presented in Table 1 [8– 11].

Parameters	Unit	W	CeB_6
Density, ρ	kg/m^3	19250	4800
Electron contribution, γ	$J/kg{\cdot}K^2$	0.022	0.813
Thermal conductivity, λ	$W/m{\cdot}K$	9680	0.94
Seebeck coefficient, S	μV/K	-	150

Table 1. Parameters of used materials

3 RESULTS

The equation of heat distribution from a limited volume in a three-dimensional model was solved for various geometries of the thermoelectric sensor with boundary conditions of absence of heat transfer to the medium and a

No.	Absorber (x,y,z),μm	Bridge (x,y,z),μm	E, eV	ΔT_{max}, 10^{-4} K	ΔU_{max}, nV	t (ΔT_{max}), ps	t (ΔT_{max}/10), ps	R, GHz
C15M	**5×0.5×0.5**	**0.01×0.5×0.5**	**100**	**21.1**	**316.5**	**3.6**	**101.1**	**9.89**
C15Ma	**5×0.5×0.5**	**0.01×0.5×0.5**	**10**	**2.11**	**31.65**	**3.9**	**101.1**	**9.89**
C15Mb	**5×0.5×0.1**	**0.01×0.5×0.1**	**10**	**11**	**165**	**3.12**	**100**	**10**
C15c	**5×0.5×0.5**	**0.01×0.5×0.5**	**1**	**0.211**	**3.165**	**3.9**	**101.1**	**9.89**
C15d	**5×0.5×0.1**	**0.01×0.5×0.1**	**1**	**1.07**	**16**	**3.81**	**101.43**	**9.86**
C16N	**5×0.5×0.5**	**0.01×0.5×0.5**	**100**	**337**	**5055**	**0.033**	**3.5**	**286**
C16Na	**5×0.5×0.5**	**0.01×0.5×0.5**	**10**	**34**	**510**	**0.03**	**3.38**	**286**
C16Nb	**5×0.5×0.1**	**0.01×0.5×0.1**	**10**	**78**	**1170**	**0.096**	**9.819**	**101.8**
C16Nc	**5×0.5×0.5**	**0.01×0.5×0.5**	**1**	**3.37**	**50**	**0.033**	**3.42**	**292.4**
C16Nd	**5×0.5×0.1**	**0.01×0.5×0.1**	**1**	**7.8**	**117**	**0.114**	**9.819**	**101.8**
C17F	**5×0.5×0.5**	**0.01×0.5×0.5**	**100**	**18.1**	**271.5**	**10.2**	**111.6**	**8.96**
C17Fa	**5×0.5×0.5**	**0.01×0.5×0.5**	**10**	**1.81**	**27**	**10.8**	**111.6**	**8.96**
C17Fb	**5×0.5×0.1**	**0.01×0.5×0.1**	**10**	**9.1**	**137**	**10.92**	**112.2**	**8.9**
C17Fc	**5×0.5×0.5**	**0.01×0.5×0.5**	**1**	**0.181**	**2.7**	**10.8**	**111.6**	**8.96**
C17Fd	**5×0.5×0.1**	**0.01×0.5×0.1**	**1**	**0.91**	**13.7**	**10.92**	**112.2**	**8.9**
C18M	**5×0.5×0.5**	**0.01×0.5×0.5**	**110**	**23.2**	**348**	**3.6**	**101.1**	**9.89**
C19M	**5×0.5×0.5**	**0.01×0.5×0.5**	**90**	**19**	**285**	**3.6**	**101.1**	**9.89**
C23M	**5×5×1.5**	**0.01×5×1.5**	**1000**	**8.54**	**130**	**2.1**	**51.3**	**19.5**
C26N	**5×5×1.5**	**0.01×5×1.5**	**1000**	**19.8**	**230**	**0.6**	**26.7**	**37.5**
C27F	**5×5×1.5**	**0.01×5×1.5**	**1000**	**8.7**	**130**	**3.9**	**52.8**	**18.9**
C28M	**5×5×1.5**	**0.01×5×1.5**	**1100**	**9.36**	**140**	**2.1**	**51**	**19.6**
C29M	**5×5×1.5**	**0.01×5×1.5**	**900**	**7.68**	**120**	**2.1**	**49.7**	**20.1**

Table 2. Sensor geometry, ΔT_{max}, ΔU_{max}, $t(\Delta T_{max}/10)$, and count rate R.

slight loss of the heat to the substrate. Table 2 shows the calculation numbers (capital letters correspond to the absorber areas with impingent photons), data on the absorber and the sensor size (x, y, z), photon energy E, maximum temperature difference $\Delta T_{\max}$ at the ends of the bridge, the time $t(\Delta T_{\max})$ in which this maximum is reached, the voltage $\Delta U_{\max}$ (calculated using the Seebeck coefficient value $S = 150$ µV/K at 9K), the time of the gradient fall to the background values $t(\Delta T_{\max}/10)$ and the detector count rate $R = 1/t(\Delta T_{\max}/10)$. As shown in [12], photons with an energy of 1 keV are absorbed with a ~ 100% probability in a 1.5 µm thick tungsten, photons with an energy of 100 eV - in a 0.5 µm thick tungsten. We can also calculate that photons with 10 eV and 1 eV energy are almost completely absorbed in the tungsten absorber with a thickness of 0.1 µm. And this thickness values for absorbers and the thermoelectric bridge is used in calculations.

Data of Table 2 will be discussed in parallel with the consideration of the time dependence of the temperature difference at the ends of the thermoelectric bridge $\Delta T(t)$. In Figure 2 these dependences are given for the absorbers with dimensions 5×5×1.5 µm^3. The insets show the number of calculations, photon energy and the sizes of the absorber and bridge.

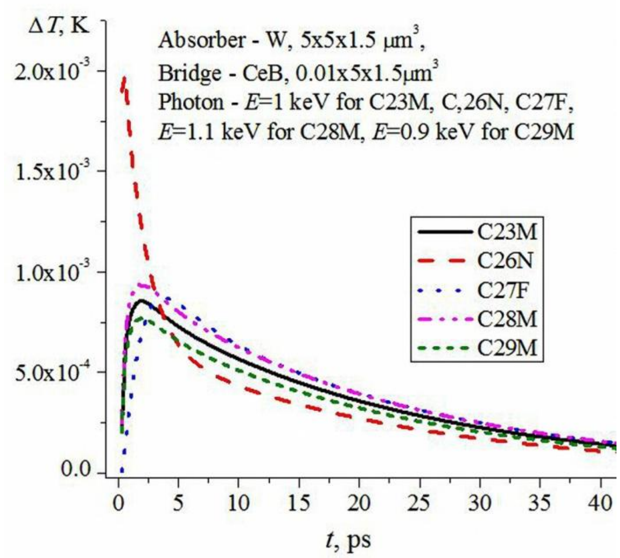

Figure 2. $\Delta T(t)$ dependence for ~1keV photon absorption.

The $\Delta T(t)$ curves significantly differ for calculations labeled M, N and F. From comparison of curves C23M and C27F (Figure 2) it is seen that photon absorption in a region far from the thermoelectric bridge of the absorber, relative to photon absorption in the center, leads to a slight increase of $\Delta T_{\max}$ and increase of $t(\Delta T_{\max})$. Let us note that calculations of C23M and C27F were done for similar values of the absorber and bridge dimensions.

Calculation C26N were also done for similar dimensions of the absorber and of the bridge; the letter N corresponds to photon absorption in vicinity of the thermoelectric bridge. In this case the time dependence of

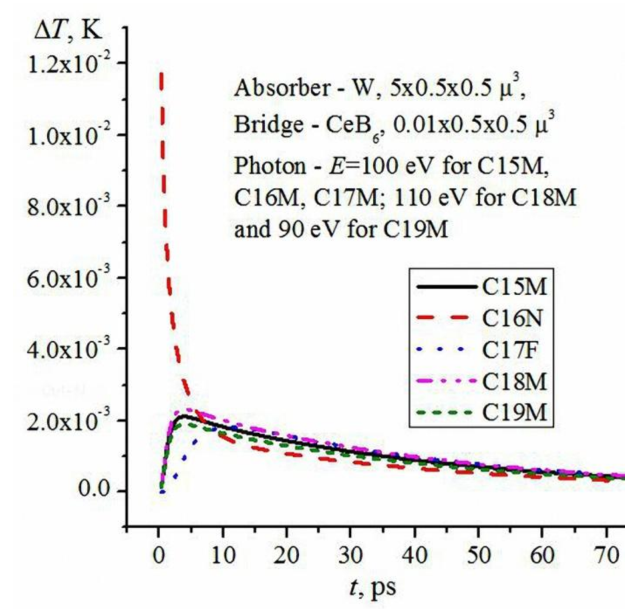

Figure 3. $\Delta T(t)$ dependence for ~100eV photon absorption.

ΔT has a different profile. As it can be seen from Figure 2, the curve C26N attains significantly higher values of ΔT in a shorter time interval. The difference between C23M and C26N disappears at t >50 ps.

If the photon energy differs by 100 eV, the $\Delta T_{\max}$ differs by 7.7 mK (C28M, C29M - Table 2). With the value of the Seebeck coefficient of 150 µV/K for CeB6 at 9 K, this provides the build-up of a ~ 10 nV voltage – a quantity that can be detected without use of special electronics. If we can measure with a high confidence the voltage of 1 nV, then we can be similarly confident in distinguishing photons of 1000±10 eV energies.

The $\Delta T(t)$ curves significantly differ for calculations labeled M, N and F also for 100eV photon absorption (Figure 3). The difference between C15M, C16N and C17F curves disappears at t > 60 ps.

If the photon energy differs by 10 eV, the $\Delta U_{\max}$ differs by 32 nV (C18M, C19M - Table 2), and the energy difference of 1 eV will generate 3.2 nV voltage. So we got a better energy resolution for 1 eV photons energy difference for the case of absorption of a photon of lower energy (1keV – 100 eV) by reducing the volume of the absorber (5×5×1.5µm^3 – 5×0.5×0.5µm^3).

The calculation results of C15Ma-C15Md are presented in Figure 4. From comparison of C15Ma, C15Mc (z=0.5µm) and C15Mb, C15Md (z=0.1µm) curves it is seen that photon absorption in detection pixel with a smaller thickness leads to the significant increase of ΔT value. As can be judged from the data of Table 2, even in the absorption of 1 eV photons, the value of the voltage more than 10 nV is obtained. We can say that a photon with this energy can be registered and its energy can be determined.

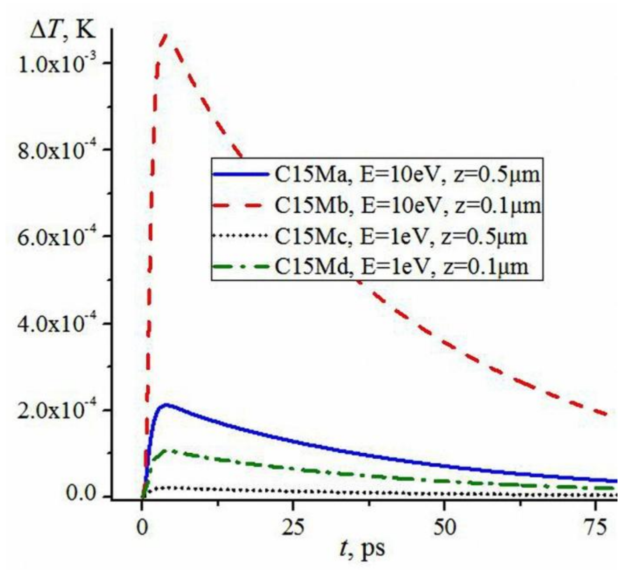

Figure 4. $\Delta T(t)$ dependence for 10eV and 1eV photon absorption in case of different thickness (z) of detection pixel.

The results of calculations show that it is realistic to detect single photons from IR to X-ray and define their energy by accuracy no less than 10%: (a) without additional amplification of the obtained signals for their registration, (b) while providing count rates exceeding 100 GHz!

If the thermoelectric bridge of CeB_6 possesses a Seebeck coefficient of S = 150 μV/K, which corresponds to the average value reported in the literature, then as can be seen in the Table 2, the resulting voltage can reach microvolts.

The obtained characteristics are encouraging, they ensure the competitiveness of the thermoelectric detector with the superconducting single-photon detectors described in the literature. The simplicity of the thermoelectric sensor design, the lack of stringent requirements for maintaining the operating temperature and the relatively high operating temperature (twice higher than the boiling point of liquid helium) are additional advantages of the thermoelectric detectors based on CeB_6.

REFERENCES

[1] R.H. Hadfield, Nat. Photonics, 3 (12), 696, 2009.
[2] K.D. Irwin, Scientific Am, 86, November 2006.
[3] T. Yamashita, S. Miki, H. Terai, and Z. Wang, Optics Express 21(22), 27177, 2013.
[4] A. Gulian, K. Wood, D. van Vechten, G. Fritz, J. Mod. Optic, 51 (9-10), 1467, 2004.
[5] A.A. Kuzanyan, A.S. Kuzanyan, Proc. of SPIE 8773, 87730L, 2013.
[6] V.A. Petrosyan, Journal of Contemporary Physics, 46 (3), 194, 2011.
[7] A.A. Kuzanyan, Nano Studies, 9, 93, 2014.
[8] T. R. Waite, R. S. Craig, W. E. Wallace, Phys. Rev., 104, 1240, 1956.
[9] http://www.efunda.com/materials/elements/TC_Table.cfm?Elment_ID=W
[10] S. R. Harutyunyan, V. H. Vardanyan, A. S. Kuzanyan, V. R. Nikoghosyan, S. Kunii, K. S. Wood, A. M. Gulian, Appl. Phys. Lett., 83, 2142, 2003.
[11] Y. Peysson, C. Ayache, B. Salce, J. Rossat–Mignod, S. Kunii, T. Kasuya. J. Magn. & Magn. Mater., 47-48, 6365, 1985.
[12] A.A. Kuzanyan, V.A. Petrosyan, A.S. Kuzanyan, Journal of Physics: Conference Series, 350, 012028, 2012.